DOI: 10.48011/asba.v2i1.1388

Design Procedure of Current Controllers for LCL-filtered Grid-Tied Inverters with Robust Stability Certification ⋆

Caio R. D. Osório[*,**], **Gustavo G. Koch**[*], **Pablo García**[***], **Vinicius F. Montagner**[*]

[*] *Federal University of Santa Maria, RS, Brazil*
[**] *Currently a visiting researcher at the University of Oviedo, Spain.*
[***] *Electrical Engineering Department, University of Oviedo, Spain*
(e-mail: caio.osorio@gmail.com)

Abstract: This paper proposes an alternative design procedure for current control of LCL-filtered grid-tied inverters, taking into account robustness against uncertain and possibly time-varying grid inductances. The control strategy is developed in stationary reference frame, and is based on a partial state feedback, including an active damping scheme of the LCL filter resonance. From the system parameters and the design specifications, analytical expressions for the calculation of the control gains are provided, oriented by a pole placement in discrete-time domain. These expressions are obtained neglecting the dynamics of the filter capacitor, including resonant controllers to track sinusoidal references, and taken into account the delay due to digital implementation. To certificate robust stability of the closed-loop system under time-varying grid inductances, a theoretical analysis based on a Lyapunov function is provided. Time and frequency domain results are presented for a case study, illustrating that the proposed design strategy is able to provide robust control gains leading to grid-injected currents with suitable responses for the entire range of grid inductances considered in the design.

Keywords: Active damping, direct pole placement, grid-tied inverter, LCL filter, robust control.

1. INTRODUCTION

Voltage source inverters are key elements in the integration of renewable energy sources to the electrical grid. Particularly, the current control loop plays an important role, being responsible to regulate the power flow between the source and the mains, besides ensuring grid currents with low harmonic distortion and suitable dynamics (Erickson, 1997; Blaabjerg et al., 2006; IEEE, 2018). Taking into account the switched nature of the inverter, low pass filters are required as interface between converter and grid, being the LCL filter widely used since it provides higher frequency attenuation and smaller size in comparison with the L filter (Poongothai and Vasudevan, 2019).

On the other hand, LCL filters have an intrinsic resonant behavior, which deteriorates the closed-loop performance and can lead to instability. Therefore, one important feature in the design of the current control loop is to ensure proper damping of the resonance peak, preferably by means of active damping approaches, what avoid the use of dissipative resistors (He et al., 2014). Moreover, one important challenge is to cope with uncertain and possibly time-varying grid impedances at the point of common coupling (PCC), which may also lead to poor performance or instability, for controllers designed only considering a nominal condition (García et al., 2018; Osório et al., 2020).

In this context, one important current control strategy is the state-feedback, that is proven capable of providing robustness and suitable dynamic performances for grid-tied inverter (GTI) with LCL filters subject to uncertain parameters (Gabe et al., 2009; Maccari et al., 2015; Kukkola et al., 2015; Osório et al., 2020). With this approach, internal model-based controllers can be taken into account and the closed-loop poles can be placed using different strategies, such as robust pole location (Osório et al., 2020), linear quadratic regulators (Maccari et al., 2015) or direct pole placement (Dannehl et al., 2010).

Considering the direct pole placement, one advantage is that the state-feedback gains can be calculated using closed-form analytical expressions, based on the system parameters and the control specifications (Kukkola et al., 2015). Moreover, to simplify the control design, a useful approach is to neglect the dynamics of the LCL filter capacitor, designing the controller based on an L filter approximation (Sivadas and Vasudevan, 2018). Instead of measuring all LCL filter states, this allows to compute the control law measuring, for instance, only the grid-injected currents, which reduce the number of sensor required for the implementation (Yin et al., 2013). However, this approach translates into a partial feedback of the LCL filter states, for which the stability is highly dependent on the damping of the physical system and parameter uncertain-

⋆ This study was financed in part by the Coordenação de Aperfeiçoamento de Pessoal de Nível Superior - Brasil (CAPES/PROEX) - Finance Code 001, INCT-GD, CNPq (465640/2014-1, 160884/2019-5 and 309536/2018-9), CAPES (23038.000776/2017-54), FAPERGS (17/2551-0000517-1), and CAPES-PRINT (88887.465639/2019-00).

ties. Thus, to ensure stability and suitable performance for the entire range of parameters, an additional active damping scheme must be included (Dannehl et al., 2009; García et al., 2018).

This paper provides an alternative procedure for the analytical design of discrete-time robust current controllers applied to GTIs with LCL filters. Closed-form expressions for calculating the state-feedback control gains are provided. The design relies on a direct pole placement based on an L filter approximation, which is modeled in stationary reference frame encompassing the digital implementation delay and resonant controllers. An active damping scheme based on the feedback of the capacitor current is included. The closed-loop system is designed taking into account robustness against uncertain grid inductances, and a certificate of robust stability under time-varying parameters, based on Lyapunov functions, is also provided. Simulation results in a realistic environment confirm that the proposed procedure provides controllers capable of ensuring suitable transient and steady-state responses for LCL-filtered GTIs, even when subject to uncertain and time-varying grid inductances.

2. MODELLING

A three-phase inverter connected to the grid by means of an LCL filter is shown in Figure 1. The grid impedance is assumed predominantly inductive, with an uncertain inductance L_{g2}.

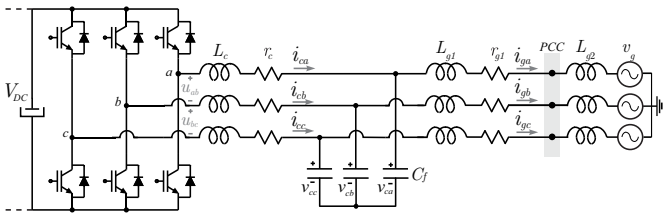

Figure 1. Three-phase LCL-filtered grid-tied inverter.

Given a balanced three-phase system, for any of the three phases, one can write that $L_g = L_{g1} + L_{g2}$, where L_g is an uncertain parameter due to the uncertainty in L_{g2}, and lies in a bounded interval given by $\mathcal{U} = [L_{gmin}, L_{gmax}]$. Note that grid resistances can be included in the modelling by simply adding it to the parameter r_{g1}.

Moreover, considering that there is no path for current circulation in axis-0, the topology in Figure 1 can be represented in stationary reference frame ($\alpha\beta$ coordinates) by two single-phase uncoupled systems, as depicted in Figure 2.

From Figure 2, the state-space model in stationary reference frame is given by

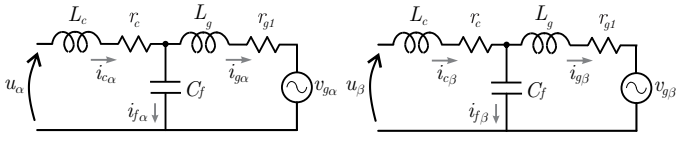

Figure 2. LCL filter model in stationary reference frame.

$$\frac{d}{dt}\begin{bmatrix} x_\alpha(t) \\ x_\beta(t) \end{bmatrix} = \begin{bmatrix} A(L_g) & 0_{3\times3} \\ 0_{3\times3} & A(L_g) \end{bmatrix}\begin{bmatrix} x_\alpha(t) \\ x_\beta(t) \end{bmatrix} + \begin{bmatrix} B_u & 0_{3\times1} \\ 0_{3\times1} & B_u \end{bmatrix}\begin{bmatrix} u_\alpha(t) \\ u_\beta(t) \end{bmatrix} + \begin{bmatrix} B_g(L_g) & 0_{3\times1} \\ 0_{3\times1} & B_g(L_g) \end{bmatrix}\begin{bmatrix} v_{g\alpha}(t) \\ v_{g\beta}(t) \end{bmatrix} \tag{1}$$

where, for the α-axis model, $x_\alpha = [i_{c\alpha}\, v_{c\alpha}\, i_{g\alpha}]'$, in which $i_{c\alpha}$ is the converter-side current, $v_{c\alpha}$ is the voltage drop across the filter capacitor and $i_{g\alpha}$ is the grid-side current. The same reasoning is valid for the β-axis model.

The matrices in (1) are given by

$$A(L_g) = \begin{bmatrix} \frac{-r_c}{L_c} & \frac{-1}{L_c} & 0 \\ \frac{1}{C_f} & 0 & -\frac{1}{C_f} \\ 0 & \frac{1}{L_g} & \frac{-r_{g1}}{L_g} \end{bmatrix},\ B_u = \begin{bmatrix} \frac{1}{L_c} \\ 0 \\ 0 \end{bmatrix},\ B_g(L_g) = \begin{bmatrix} 0 \\ 0 \\ -\frac{1}{L_g} \end{bmatrix} \tag{2}$$

Notice that under the assumption that the system is balanced, the exact same representation is obtained for the α and β axes. Thus, from this point on, these subscripts will be omitted, and the equations are valid for both axes.

For the implementation of a digital control strategy in a digital signal processor (DSP), the discretized model of the plant can be written as

$$\begin{aligned} x(n+1) &= A_d(L_g)\cdot x(n) + B_{ud}(L_g)\cdot u(n) + B_{gd}(L_g)\cdot v_g(n) \\ y(n) &= C\cdot x(n) = i_g(n), \quad C = [\,0\ 0\ 1\,] \end{aligned} \tag{3}$$

where $x(n) = [i_c(n)\, v_c(n)\, i_g(n)]'$.

From (2), for a given sampling period T_s, the matrices in (3) are given by

$$\begin{aligned} A_d(L_g) &= e^{A(L_g)\cdot T_s},\ B_{ud}(L_g) = \int_0^{T_s} e^{A(L_g)\cdot\tau}\cdot B_u\cdot d\tau, \\ B_{gd}(L_g) &= \int_0^{T_s} e^{A(L_g)\cdot\tau}\cdot B_g(L_g)\cdot d\tau \end{aligned} \tag{4}$$

The Problem to be solved in this paper is defined as: given the LCL filter with model in (3), find a robust controller (fixed control gains) that: i) ensures stability under uncertain and possibly time-varying grid inductances; ii) ensures tracking of sinusoidal references for grid injected currents and rejection of harmonic disturbances; iii) copes with digital implementation delay of the controller.

2.1 Case Study

The system parameters for a case study are shown in Table 1, where the LCL filter parameters are borrowed from García et al. (2018). The grid inductance is defined withing a large interval to better investigate the effects of the inductance variation on the system performance.

3. PARTIAL STATE FEEDBACK CONTROL

In this Section, an analytical design procedure for a partial state feedback control is proposed. The control strategy is based on the feedback of the grid current, and the design is carried out neglecting the dynamics of the filter capacitor. Thus, the LCL filter described in (1) is approximated by

Table 1. System Parameters

Parameter	Value
L_c, C_f and L_{g1}	2.3 mH, 10 μF and 0.93 mH
r_c and r_{g1}	0.2 mΩ and 0.2 mΩ
Grid inductance L_{g2}	[0 mH, 5 mH]
DC-ling voltage (V_{DC})	400 V
Grid phase voltage	127 V(rms); 50 Hz
Sampling Frequency	16 kHz
Switching Frequency	8 kHz

an L filter, with an equivalent resistance given by $R_t = r_c + r_{g1}$, and an equivalent inductance given by $L_t = L_c + L_g$, with $L_g \in \mathcal{U}$ being an uncertain parameter.

In stationary reference frame, the dynamic equation of the three-phase L filter approximation can be written as

$$\frac{d}{dt} i_g(t) = -\frac{R_t}{L_t} i_g(t) + \frac{1}{L_t} u(t) - \frac{1}{L_t} v_g(t) \tag{5}$$

which is valid for both α and β axes.

The discretized model is given by

$$\begin{aligned} i_g(n+1) &= A_L(L_g)\cdot i_g(n) + B_{uL}(L_g)\cdot u(n) + B_{gL}(L_g)\cdot v_g(n) \\ y_L(n) &= i_g(n) \end{aligned} \tag{6}$$

where, considering a sufficiently small sampling period T_s and using, for instance, Euler Approximation, one has that $A_L = 1 - T_s R_t/L_t$, $B_{uL} = T_s/L_t$ and $B_{gL} = -T_s/L_t$.

In order to track sinusoidal grid current references and to reject disturbances from the grid voltage, consider now the inclusion of a resonant controller at a frequency ω_r. In continuous-time domain, the state-space model of this controller is given by

$$\frac{d}{dt}\begin{bmatrix}\zeta_1(t)\\ \zeta_2(t)\end{bmatrix} = \begin{bmatrix} 0 & 0 \\ -\omega_r & -2\cdot\xi_r\cdot\omega_r \end{bmatrix}\begin{bmatrix}\zeta_1(t)\\ \zeta_2(t)\end{bmatrix} + \begin{bmatrix}0\\1\end{bmatrix}(r(t) - i_g(t)) \tag{7}$$

where $\zeta_1(t)$ and $\zeta_2(t)$ are the internal states, ξ_r is the damping factor, and $r(t)$ is the reference for the grid currents.

From the discretization of (7), a state space discrete-time representation for this resonant controller is given by

$$\begin{bmatrix}\zeta_1(n+1)\\ \zeta_2(n+1)\end{bmatrix} = \begin{bmatrix} R_{11} & R_{12} \\ R_{21} & R_{22} \end{bmatrix}\begin{bmatrix}\zeta_1(n)\\ \zeta_2(n)\end{bmatrix} + \begin{bmatrix}T_1\\T_2\end{bmatrix}(r(n) - i_g(n)) \tag{8}$$

Considering now the plant in (6), the resonant controller in (8), and including a state $\phi(n)$, to represent the control delay in the digital implementation, the augmented model of the L filter approximation can be written as

$$\begin{aligned} \begin{bmatrix} i_g(n+1)\\ \phi(n+1)\\ \zeta_1(n+1)\\ \zeta_2(n+1)\end{bmatrix} &= \begin{bmatrix} A_L(L_g) & B_{uL}(L_g) & 0 & 0 \\ 0 & 0 & 0 & 0 \\ -T_1 & 0 & R_{11} & R_{21} \\ -T_2 & 0 & R_{21} & R_{22}\end{bmatrix}\begin{bmatrix} i_g(n)\\ \phi(n)\\ \zeta_1(n)\\ \zeta_2(n)\end{bmatrix} \\ &+ \begin{bmatrix}0\\1\\0\\0\end{bmatrix}u(n) + \begin{bmatrix}0\\0\\T_1\\T_2\end{bmatrix}r(n) + \begin{bmatrix}B_{gL}(L_g)\\0\\0\\0\end{bmatrix}v_g(n) \end{aligned} \tag{9}$$

which, in a more compact form, is given by

$$\begin{aligned} \rho_L(n+1) &= G_L\cdot\rho_L(n) + H_{uL}\cdot u(n) + H_{rL}\cdot r(n) + H_{gL}\cdot v_g(n) \\ y(n) &= C_L\cdot\rho_L(n) = i_g(n), \;\; C_L = [\,1\;0\;0\;0\,] \end{aligned} \tag{10}$$

3.1 Control Design - Feedback of the Grid-Side Current

Based on the L filter approximation in (10), consider the state-feedback control law given by

$$u_L(n) = -K_L\cdot\rho_L(n) = -\,[\,k_{ig}\;\; k_d\;\; k_{r1}\;\; k_{r2}\,]\begin{bmatrix} i_g(n)\\ \phi(n)\\ \zeta_1(n)\\ \zeta_2(n)\end{bmatrix} \tag{11}$$

Replacing the control law (11) in (10) leads to the closed-loop system

$$\rho_L(n+1) = (G_L - H_{uL}\cdot K_L)\,\rho_L(n) + H_{rL}\cdot r(n) + H_{gL}\cdot v_g(n) \tag{12}$$

From (12), considering the grid-voltage as an external disturbance and making $v_g(n) = 0$, the transfer function from the reference $r(n)$ to the output $i_g(n)$ can be written as

$$\frac{i_g(z)}{r(z)} = C_L(z\cdot I - (G_L - H_{uL}\cdot K_L))^{-1} H_r \tag{13}$$

where the characteristic polynomial (i.e., the denominator) is given by

$$P_L(z) = \det(z\cdot I - G_L + H_{uL}\cdot K_L) \tag{14}$$

Notice that, for time-invariant systems with precisely known parameters, if the system is controllable, a gain vector K_L can be calculated such that $P_L(z)$ is equal to a target characteristic polynomial, given by

$$\begin{aligned} Q(z) &= (z-\delta_1)(z-\delta_2)(z-\delta_3)(z-\delta_4) \\ &= z^4 + Q_3 z^3 + Q_2 z^2 + Q_1 z + Q_0 \end{aligned} \tag{15}$$

This polynomial $Q(z)$ allocates the closed-loop poles in arbitrary positions defined by the designer (i.e., δ_1, δ_2, δ_3 and δ_4), setting the desired closed-loop dynamics.

To accomplish that, the gain vector K_L can be calculate using numerical tools, such as the command *place*, in MATLAB. On the other hand, analytical expressions for the gains computation is a matter of interest, since enable, for instance, on-line computation of the gains, useful in adaptive control strategies.

One efficient way to provide closed-form expressions for the calculation of K_L is using Ackermann's formula (Dorf and Bishop, 2008). For the particular fourth-order system in (9)-(10), the gain vector K_L is given by

$$K_L = \mathcal{M}\cdot\mathcal{C}^{-1}\cdot\psi \tag{16}$$

where,

$$\begin{aligned} &\mathcal{M} = [\,0\;0\;0\;1\,] \\ &\mathcal{C} = \left[\,H_{uL}\;\; G_L\cdot H_{uL}\;\; {G_L}^2\cdot H_{uL}\;\; {G_L}^3\cdot H_{uL}\,\right] \\ &\psi = {G_L}^4 + Q_3\cdot{G_L}^3 + Q_2\cdot{G_L}^2 + Q_1\cdot G_L + Q_0\cdot I \end{aligned} \tag{17}$$

with G_L and H_{uL} given in (10), and Q_3, Q_2, Q_1 and Q_0 being the coefficients of the desired characteristic polynomial, as given in (15).

The closed-form analytical expressions for the calculation of the gains are given in Appendix A.

Remark 1: Notice that $\mathcal{C}$ is the controlability matrix of the system (10). Thus, if the system is controllable, $\mathcal{C}$ is invertible and there is a gain vector K_L that allocate the closed-loop poles as defined by the desired characteristic polynomial. On the other hand, although the closed-loop

poles can be set arbitrarily, due to constrains such as control saturation and limited bandwidth, there is no guarantee that the resulting gain K_L would lead to a control action viable in practice. Thus, a tradeoff between dynamic performance and control effort must be taken into account when choosing the poles location.

Remark 2: The design of fixed control gains will be investigated here, and not an adaptive strategy. In this context, since the grid inductances are assumed to be uncertain parameters, it is not possible to place the poles in the exact same positions for the entire range of parameters, and a nominal condition must be chosen to design the control gains. Thus, a trade-off between robustness and dynamic performance must also be taken into account when choosing the poles location. A similar reasoning is valid if uncertain grid resistances are considered in the design.

Based on what was stated in the *Remark 1*, Subsection 3.2 provides a procedure for the choice of the pole location.

Considering what was stated in *Remark 2*, it is proposed here to design the controller for a nominal condition given by $L_g = L_{gmin}$. Although the controller is being designed using an L filter approximation, the actual application is the LCL filter depicted in Figure 1. In this way, considering the LCL resonance frequency, the minimum grid inductance represents the condition with higher resonance frequency.

3.2 Criteria for Pole Location

Based on the L filter approximation, to define the closed-loop poles location of the system (10), the following strategy is proposed here:

i) In continuous-time, consider that a pair of complex poles is chosen to set the dominant dynamics of the closed-loop system, given by
$$s^2 + 2\cdot\xi_{dom}\cdot\omega_{dom}\cdot s + {\omega_{dom}}^2 \tag{18}$$
The parameter ξ_{dom} is the damping ratio, and can be set close to 1 in order to avoid oscillations or large overshoots. Parameter ω_{dom} can be chosen based on the desired bandwidth of the system. After defining the desired dynamics, the discrete poles are given by
$$\delta_{1,2} = e^{\left(-\xi_{dom} \pm j\sqrt{1-{\xi_{dom}}^2}\right)\cdot\omega_{dom}\cdot T_s} \tag{19}$$
Notice that if $\delta_{1,2}$ are the dominant poles, then the modulus $|\delta_{1,2}|$ defines a limitation for the decay ratio of the closed-loop transient responses.

ii) The third pole is set to $\delta_3 = 0$, originated from the delay due to the digital implementation.

iii) The fourth pole, δ_4, is set as a real pole, with a value slightly lower than the modulus $|\delta_{1,2}|$. This choice avoid higher control gains, but also keeping the limit for the decay ratio of the closed-loop transient responses given by $\delta_{1,2}$.

Considering the case study with parameters in Table 1, model in (10) is computed for $L_{g2} = 0$ mH and including a resonant controller tuned at 50 Hz, with a damping factor of 0.0001.

Following the steps provided in Section 3.2, the pole location is defined for $\omega_{dom} = 350$ Hz and $\xi_{dom} = 0.9$, leading to $\delta_{1,2} = 0.882059 \pm j\ 0.052908$, $\delta_3 = 0$ and $\delta_4 = 0.88$. Given these poles, the coefficients of the characteristic polynomial (Q_3, Q_2, Q_1, Q_0) are obtained from (15), and then the control gains are computed using the equations (A.1)-(A.4), in the Appendix, leading to

$$K_L = [\,20.132019\ \ 0.347752\ \ 153.276571\ \ 147.154611\,] \tag{20}$$

For a sweep in the uncertain parameter L_g, from $L_{gmin} = 0.93$ mH to $L_{gmax} = 5.93$ mH, Figure 3 shows the closed-loop poles of the L filter approximation in (10), with controller (11) and gains in (20). All poles are inside the unit circle, indicating stability for the entire range of parameters. Moreover, the desired pole location is depicted by red squares. When the design condition matches the uncertain parameter (i.e. $L_g = L_{gmin}$), the poles are allocated exactly at the desired positions. As the actual value of L_g diverges from the nominal condition, the poles are shifted towards the edge of the unit circle, which tends to reduce the dynamic performance.

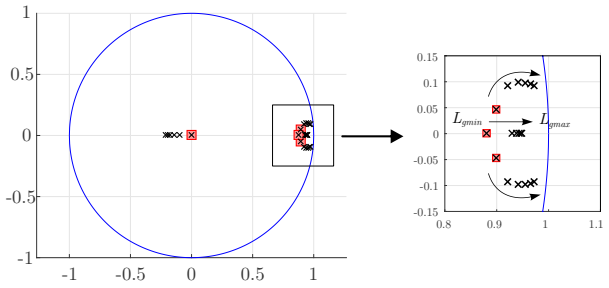

Figure 3. Closed-loop poles for a sweep in L_g: L filter approximation (10), with control law (11) and gains in (20).

It is important to mention that the choices of the pole location for this case study were made considering a trade-off between robustness and performance under uncertain grid inductances, for the interval given in Table 1. If this interval had closer bounds or, ideally, if the grid inductance was precisely known, the specifications could be improved to achieve higher dynamic performance.

4. RESPONSES OF THE LCL FILTER WITH PARTIAL STATE FEEDBACK CONTROLLER

The control design procedure in Section 2 is based on an L filter approximation. In this section, the responses of the actual LCL filter will be evaluated.

From the model in (3) and considering the control law (11), the augmented closed-loop system of the LCL filter, including the resonant controller and the digital implementation delay, is given by

$$\begin{bmatrix} x(n+1) \\ \phi(n+1) \\ \zeta_1(n+1) \\ \zeta_2(n+1) \end{bmatrix} = \begin{bmatrix} A_d(L_g) & B_{ud}(L_g) & 0_{3\times1} & 0_{3\times1} \\ K_x & -k_d & -k_{r1} & -k_{r2} \\ -T_1\cdot C & 0 & R_{11} & R_{12} \\ -T_2\cdot C & 0 & R_{21} & R_{22} \end{bmatrix} \begin{bmatrix} x(n) \\ \phi(n) \\ \zeta_1(n) \\ \zeta_2(n) \end{bmatrix} + \begin{bmatrix} 0_{3\times1} \\ 0 \\ T_1 \\ T_2 \end{bmatrix} r(n) + \begin{bmatrix} B_{gd}(L_g) \\ 0 \\ 0 \\ 0 \end{bmatrix} v_g(n) \tag{21}$$

where $x(n) = [i_c(n)\, v_c(n)\, i_g(n)]'$ and $K_x = [\,0\ 0\ k_{ig}\,]$.

Given the model (21), with parameters from the case study (Table 1) and control gains in (20), Figure 4 shows the closed-loop poles for a sweep in the uncertain parameter L_g, from L_{gmin} to L_{gmax}. This figure shows that when the actual LCL filter is taken into account, the poles related to the inherent resonance of the filter are placed outside the unit circle, leading to an unstable closed-loop system.

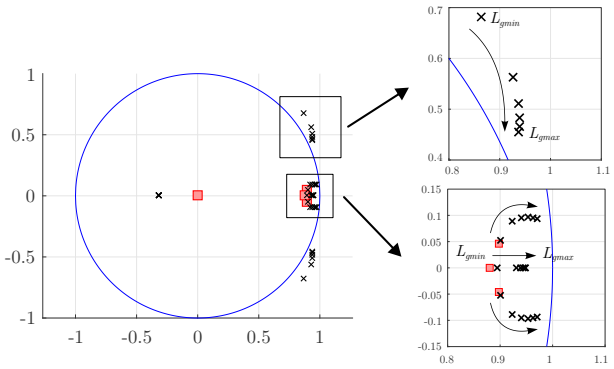

Figure 4. Closed-loop poles for a sweep in L_g: LCL filter model in (21), with control gains in (20).

This behavior is expected since the control design was based on an L filter approximation, which is not suitable for all sets of LCL filter parameters. Therefore, when the grid-side current is the only state being feedback, a damping strategy is usually required to enable stable operation with suitable dynamics under the LCL resonance.

4.1 Modified Control Law - Active Damping

To provide active damping of the LCL filter resonance, consider the feedback of the capacitor current i_f, given by

$$u_{ad}(n) = k_{ad} \cdot i_f(n) = k_{ad} \cdot (i_c(n) - i_g(n)) \tag{22}$$

where u_{ad} is an additional parcel of the control law, related to the active damping, and k_{ad} is the respective gain.

From the control law (11), but now including the active damping in (22), one has that the modified control law applied to the LCL filter is given by

$$u_{LCL}(n) = u_L(n) + u_{ad}(n) \tag{23}$$

The closed-loop system considering the model in (21) and the modified control law in (23) is given by

$$\begin{bmatrix} x(n+1) \\ \phi(n+1) \\ \zeta_1(n+1) \\ \zeta_2(n+1) \end{bmatrix} = \begin{bmatrix} A_d(L_g) & B_{ud}(L_g) & 0_{3\times1} & 0_{3\times1} \\ K_m & -k_d & -k_{r1} & -k_{r2} \\ -T_1 \cdot C & 0 & R_{11} & R_{12} \\ -T_2 \cdot C & 0 & R_{21} & R_{22} \end{bmatrix} \begin{bmatrix} x(n) \\ \phi(n) \\ \zeta_1(n) \\ \zeta_2(n) \end{bmatrix} + \begin{bmatrix} 0_{3\times1} \\ 0 \\ T_1 \\ T_2 \end{bmatrix} r(n) + \begin{bmatrix} B_{gd}(L_g) \\ 0 \\ 0 \\ 0 \end{bmatrix} v_g(n) \tag{24}$$

where

$$K_m = [\, k_{ad} \quad 0 \quad -(k_{ig} + k_{ad}) \,]$$

and the gains k_{ig}, k_d, k_{r1} and k_{r2} are designed with the procedure proposed in Section 3.

System (24) can be written in a more compact form as

$$\begin{aligned} \rho(n+1) &= G_{\text{mf}}(L_g) \cdot \rho(n) + H_r \cdot r(n) + H_g \cdot v_g(n) \\ y(n) &= C_{aug} \cdot \rho(n) = i_g(n), \quad C_{aug} = [\, 0 \; 0 \; 1 \; 0 \; 0 \; 0 \,] \end{aligned} \tag{25}$$

The design of the active damping gain can be done by analysing the closed-loop poles of the system (24), for different choices of k_{ad}.

Considering the proposed control design strategy, the damping gain should be negative in order to have stable operation. Moreover, the modulus of k_{ad} must be large enough so that all closed-loop poles remain inside the unit circle for the entire range of $L_g \in \mathcal{U}$. On the other hand, a limitation on the modulus of k_{ad} must be considered in order to minimize the control effort, since increasing excessively its modulus leads to an increase in the natural frequency of the filter resonance.

Taking into account these considerations, the active damping gain chosen for the case study with parameters in Table 1 is given by

$$k_{ad} = -20 \tag{26}$$

Considering (24), with control gains in (20) and damping gain in (26), the closed-loop poles of the system is shown in Figure 5, for a sweep in the uncertain parameter L_g, from L_{gmin} to L_{gmax}. Differently from Figure 4, all closed-loop poles are now inside the unit circle, indicating stability for the entire range of L_g.

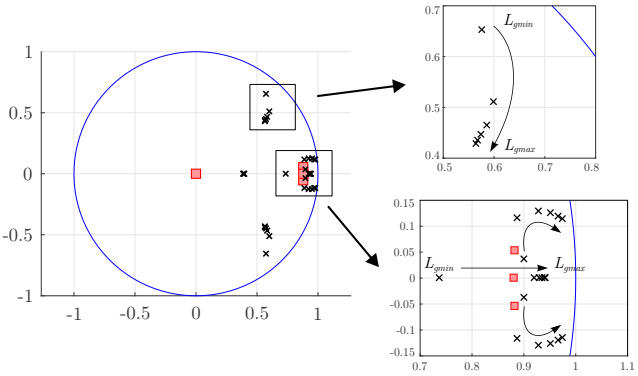

Figure 5. Closed-loop poles for a sweep in L_g: LCL filter model (24), with control gains in (20) and (26).

To confirm the capacity of this closed-loop system to track sinusoidal references, Figure 6(a) shows the frequency responses from the reference to the output, for a sweep in L_g, from L_{gmin} to L_{gmax}. It possible to verify gain equal to 0 dB at the frequency $2\pi50$ rad/s, which ensures tracking of sinusoidal references at this frequency. The capacity to reject disturbances from the grid voltage is confirmed in the Bode diagram show in Figure 6(b), where it possible to verify attenuation in the entire frequency range.

Figure 7(a) and (b) show the closed-loop responses for a reference variation test performed with the extreme values of the uncertain parameter. It is possible to verify that the closed-loop system is able to track the grid current reference with suitable transient and steady state performances, for both extreme values of the grid inductance.

Remark 3: Notice that the design of k_{ad} relies on the desired pole location, as defined in Section 3.2. If the desired pole location impairs the design of a suitable active damping (i.e. if it is not possible to stabilize the system for the entire range of parameters), thus the tradeoff between robustness and performance must be reconsidered, and

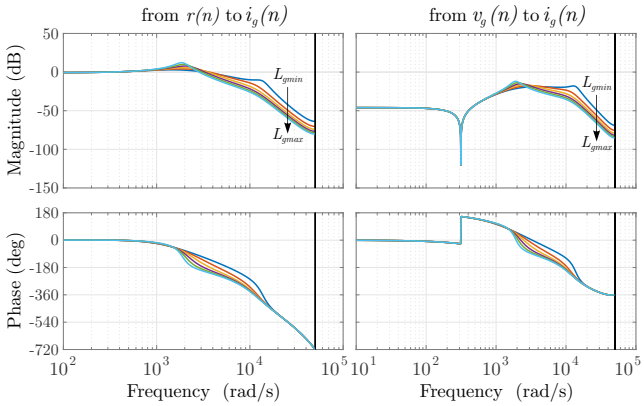

(a) (b)

Figure 6. Closed-loop frequency responses for a sweep in L_g: (a) from the reference to the output; (b) from the disturbance to the output.

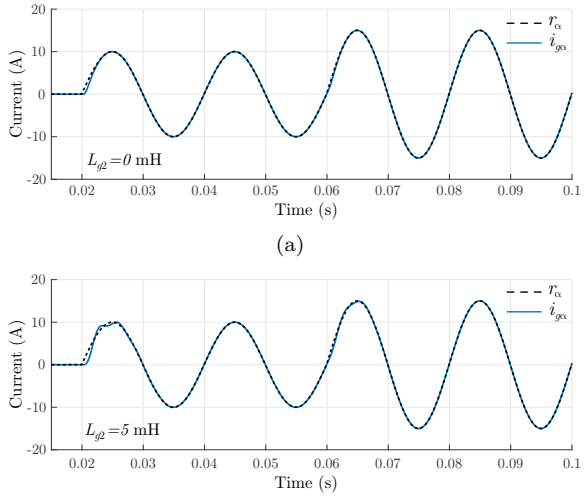

(a)

(b)

Figure 7. Closed-loop responses for a reference variation test with: (a) $L_{g2} = 0$ mH; (b) (a) $L_{g2} = 5$ mH

the pole location must be relaxed by reducing the desired bandwidth or the damping of the system.

Remark 4: Notice that for the computation of (23), besides the grid-side current (i_g), the only additional state required is the converter-side (i_c) current, which is reasonable considering that this measurement is usually available in industrial inverters for protection purposes. Thus, the control strategy presented in Section 3 requires less sensors then a full state feedback control, demanding the same amount of measurements then a classical PI controller with the same active damping scheme.

5. CERTIFICATE OF ROBUST STABILITY UNDER TIME-VARYING PARAMETERS

The analysis of the closed-loop poles shown in Figure 5 provides a robust stability indicative for the system in (24)–(25), taking into account uncertain but time-invariant grid inductances. In this context, it is important to provide a theoretical certificate of stability valid for any value of L_g lying in a given bounded interval, encompassing arbitrarily fast variation of this parameter over time.

The stability of the closed-loop system (25) can be analyzed by means of the asymptotic stability of the polytopic system given by (Boyd et al., 1994)

$$\rho(n+1) = G_{\text{mf}}(\theta(n))\cdot\rho(n), \tag{27}$$

with

$$G_{\text{mf}}(\theta(n)) = \theta(n)\cdot G_{\text{mf1}} + (1-\theta(n))\cdot G_{\text{mf2}} \tag{28}$$

for all real values of $\theta(n)$, with $0 \leq \theta(n) \leq 1$, and vertices given by

$$G_{\text{mf1}} = G_{\text{mf}}(L_{gmin}) \quad \text{and} \quad G_{\text{mf2}} = G_{\text{mf}}(L_{gmax}) \tag{29}$$

The time-variant system (27) is asymptotically stable if there is a matrix $P = P' > 0$, such that

$$G_{\text{mf}i}{}'\cdot P\cdot G_{\text{mf}i} - P < 0, \quad \text{for} \quad i = 1, 2 \tag{30}$$

This result is based on a Lyapunov function given by $v(\rho(n)) = \rho(n)'\cdot P\cdot\rho(n)$, which certifies the stability of the closed-loop system for slow or arbitrary fast parametric variations over time.

For the case study, verifying the feasibility of (30) for the vertices (29) and gains in (20) and (26), there is solution P for the problem with $L_{g2} \in [0$ mH, 4.7 mH], which certifies closed-loop stability for uncertain but also time-variant grid inductances lying in this interval.

6. RESULTS

The results shown in this section were obtained using the software PSIM. The LCL-filtered grid-tied inverter depicted in Figure 1 was simulated with the parameters on Table 1. The control algorithm was written in C language, with syntax compatible with DSP implementation. The converter-side and grid-side currents are measured (*abc* coordinates) and, after analog to digital conversion, are transformed to $\alpha\beta$ coordinates using the Clarke transformation. The control law is digitally implemented based on (23), with gains in (20) and (26). A space vector modulation is used to drive the inverter switches. The synchronism of the grid currents with voltage ate the point of common coupling (PCC) is ensured by a Kalman Filter algorithm (Cardoso et al., 2008).

To verify the closed-loop performance subject to uncertain grid inductances, tests under grid current reference variations are performed. Considering injection of active power into the grid, in the instant $t = 0.02$ s, the reference is changed from 0 A to 10 A (peak), and in $t = 0.06$ s the reference is changed from 10 A to 20 A (peak). Figure 8 shows the current-responses in $\alpha\beta$ coordinates for the system operating with L_{gmin} (i.e. $L_{g2} = 0$ mH), while Figure 9 shows the current-responses with L_{gmax} (i.e. $L_{g2} = 5$ mH).

Figure 8 and Figure 9 confirm stable responses for both extreme values of the grid inductance, with overall suitable transient and steady state performances as expected by the analysis of the closed-loop poles in Figure 5 and the frequency responses in Figure 6. When compared to the nominal condition chosen for the design (L_{gmin}), the closed-loop responses with the maximum grid inductance exhibit a deteriorated transient performance. This outcome is expected in view of the need to guarantee robustness with fixed gains for a wide range of parameters.

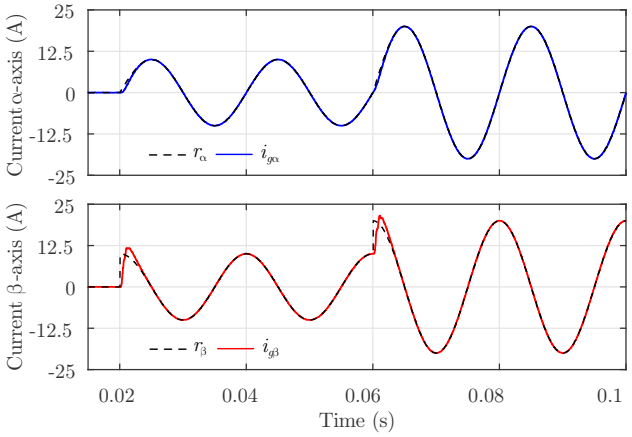

Figure 8. Currents in α-axis (top) and β-axis (bottom) for a reference variation test with $L_{g2} = 0$ mH.

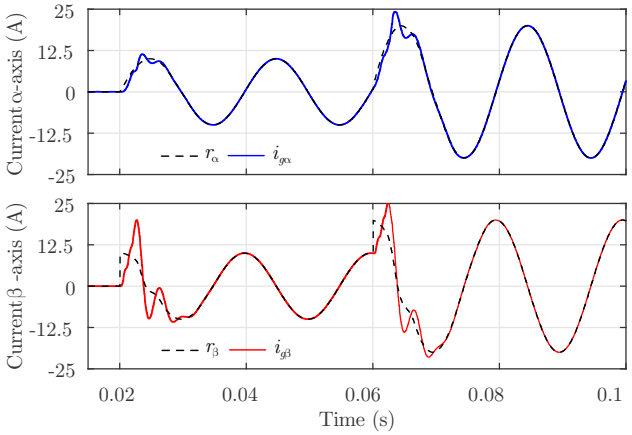

Figure 9. Currents in α-axis (top) and β-axis (bottom) for a reference variation test with $L_{g2} = 5$ mH.

Figure 10(a) and (b) show the three-phase grid currents in *abc* coordinates with respect to the $\alpha\beta$ currents shown in Figure 8 and Figure 9, respectively. These results confirm that the proposed control design leads to a robust closed-loop system, with suitable transient and steady state performances for the entire range of parameters.

The analysis presented in Section 5 certifies robust stability against arbitrarily fast variation of the grid inductance, lying in the interval [0 mH, 4.7 mH]. To confirm that, Figure 11 shows the responses of the grid currents, in $\alpha\beta$ coordinates, under switching of the grid inductance from 0 mH to 4.7 mH, at $t = 0.05$ s, and from 4.7 mH to 0 mH, at $t = 0.08$ s.

Figure 12 shows the three-phase grid currents, in *abc* coordinates, with respect to the $\alpha\beta$ currents shown in Figure 11. This results confirm stability under time-varying parameters, with suitable transient and steady-state responses.

7. CONCLUSION

This paper proposed a design procedure of current controllers applied to LCL-filtered grid-tied inverters. The procedure is based on analytical expressions for calculation of the control gains, ensuring suitable closed-loop pole

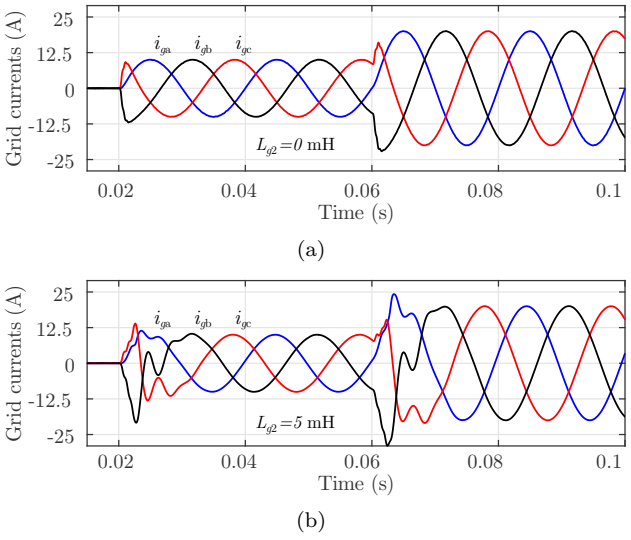

Figure 10. Three-phase grid currents for the reference variation test with: (a) $L_{g2} = 0$ mH; (b) $L_{g2} = 5$ mH.

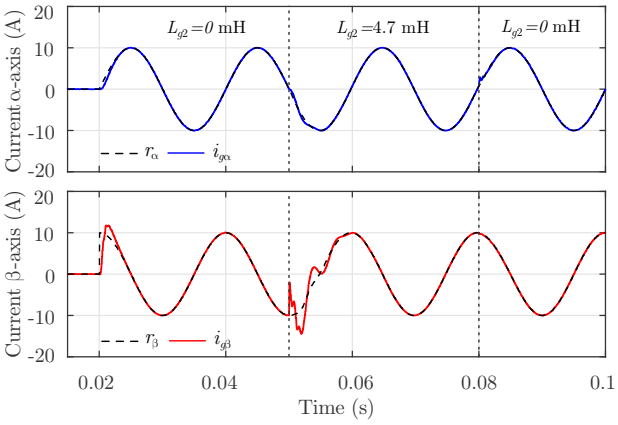

Figure 11. Currents in α-axis (top) and β-axis (bottom) under switching of the grid inductances.

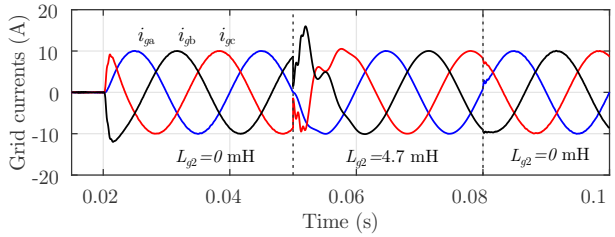

Figure 12. Three-phase grid currents under switching of the grid inductances.

location in discrete-time domain, encompassing the delay in digital control implementation, resonant controllers and operation with uncertain grid inductances. The stability of the closed-loop system against time-varying parameters is ensured by linear matrix inequalities, based on a Lyapunov function. The control gains obtained with the proposed procedure are evaluated in PSIM simulations, ensuring good performances for the closed-loop systems. One advantage of the direct pole placement is that the state-feedback gains can be calculated in an efficient way, from the system parameters and the control specifications, using closed-form analytical expressions. This enables, for

instance, automatic tuning of the controllers and, also online adaptation of the gains, which is an interesting feature to be explored in future works.

REFERENCES

Blaabjerg, F., Teodorescu, R., Liserre, M., and Timbus, A. (2006). Overview of control and grid synchronization for distributed power generation systems. *IEEE Transactions on Industrial Electronics*, 53(5), 1398 –1409.

Boyd, S., El Ghaoui, L., Feron, E., and Balakrishnan, V. (1994). *Linear Matrix Inequalities in System and Control Theory*. SIAM Studies in Applied Mathematics, Philadelphia, PA.

Cardoso, R., de Camargo, R.F., Pinheiro, H., and Gründling, H.A. (2008). Kalman filter based synchronisation methods. *IET Generation, Transmission Distribution*, 2(4), 542–555.

Dannehl, J., Fuchs, F., and Thøgersen, P. (2010). PI state space current control of grid-connected PWM converters with LCL filters. *IEEE Transactions on Power Electronics*, 25(9), 2320 –2330.

Dannehl, J., Wessels, C., and Fuchs, F. (2009). Limitations of voltage-oriented PI current control of grid-connected PWM rectifiers with filters. *IEEE Transactions on Industrial Electronics*, 56(2), 380 –388.

Dorf, R.C. and Bishop, R.H. (2008). *Modern control systems*. Prentice Hall, Upper Saddle River, USA, 11 edition.

Erickson, R.W. (1997). *Fundamentals of Power Electronics*. Chapman & Hall, New York, NY.

Gabe, I.J., Montagner, V.F., and Pinheiro, H. (2009). Design and implementation of a robust current controller for VSI connected to the grid through an LCL filter. *IEEE Transactions on Power Electronics*, 24(6), 1444–1452.

García, P., Sumner, M., Navarro-Rodríguez, ., Guerrero, J.M., and García, J. (2018). Observer-based pulsed signal injection for grid impedance estimation in three-phase systems. *IEEE Transactions on Industrial Electronics*, 65(10), 7888–7899.

He, Y., Wang, K., and Chung, H.S. (2014). Utilization of proportional filter capacitor voltage feedforward to realize active damping for digitally-controlled grid-tied inverter operating under wide grid impedance variation. In *2014 IEEE Energy Conversion Congress and Exposition (ECCE)*, 4450–4457.

IEEE (2018). IEEE standard for interconnection and interoperability of distributed energy resources with associated electric power systems interfaces. *IEEE Std 1547-2018 (Revision of IEEE Std 1547-2003)*, 1–138.

Kukkola, J., Hinkkanen, M., and Zenger, K. (2015). Observer-based state-space current controller for a grid converter equipped with an LCL filter: Analytical method for direct discrete-time design. *IEEE Transactions on Industry Applications*, 51(5), 4079–4090.

Maccari, L.A., Santini, C.L.A., Pinheiro, H., Oliveira, R.C.L.F., and Montagner, V.F. (2015). Robust optimal current control for grid-connected three-phase pulse-width modulated converters. *IET Power Electronics*, 8(8), 1490–1499.

Osório, C.R.D., Koch, G.G., Pinheiro, H., Oliveira, R.C.L.F., and Montagner, V.F. (2020). Robust current control of grid-tied inverters affected by LCL filter soft-saturation. *IEEE Transactions on Industrial Electronics*, 67(8), 6550–6561.

Poongothai, C. and Vasudevan, K. (2019). Design of LCL filter for grid-interfaced pv system based on cost minimization. *IEEE Transactions on Industry Applications*, 55(1), 584–592.

Sivadas, D. and Vasudevan, K. (2018). Stability analysis of three-loop control for three-phase voltage source inverter interfaced to the grid based on state variable estimation. *IEEE Transactions on Industry Applications*, 54(6), 6508–6518.

Yin, J., Duan, S., and Liu, B. (2013). Stability analysis of grid-connected inverter with LCL filter adopting a digital single-loop controller with inherent damping characteristic. *IEEE Transactions on Industrial Informatics*, 9(2), 1104–1112.

Appendix A. ANALYTICAL EXPRESSIONS FOR CONTROL GAIN VECTOR COMPUTATION

From the Ackermann's formula, solving (16), the closed-form analytical expressions for the computation of the entries of the vector K_L, in (11), are given by

$$k_{ig} = \frac{Q_2 + Q_3\left(A_{dL} + f_0\right) + {A_{dL}}^2 + A_{dL} f_0 + f_2 + f_4 + {R_{11}}^2 + {R_{22}}^2}{B_{udL}} \tag{A.1}$$

$$k_d = Q_3 + A_{dL} + R_{11} + R_{22} \tag{A.2}$$

$$k_{r1} = \frac{a_0 Q_0 + a_1 Q_1 + a_2 Q_2 + \left(a_{3a} + a_{3b}\right) Q_3 + \left(a_{4a} + a_{4b}\right) Q_4}{a_{div}} \tag{A.3}$$

$$k_{r2} = \frac{b_0 Q_0 + b_1 Q_1 + b_2 Q_2 + \left(b_{3a} + b_{3b}\right) Q_3 + \left(b_{4a} + b_{4b}\right) Q_4}{b_{div}} \tag{A.4}$$

with auxiliary parameters given by

$$\begin{aligned} &f_0 = R_{11} + R_{22},\ f_1 = R_{11}R_{21},\ f_2 = R_{12}R_{21},\ f_3 = R_{21}R_{22} \\ &f_4 = R_{11}R_{22},\ f_5 = R_{11}R_{12},\ f_6 = R_{12}R_{22} \end{aligned} \tag{A.5}$$

The parameters for the calculation of k_{r1}, in (A.3), are given by

$$\begin{aligned} a_0 &= -T_2, \\ a_1 &= T_1 R_{21} - T_2 R_{11}, \\ a_2 &= T_1\left(f_1 + f_3\right) - T_2\left({R_{11}}^2 + f_2\right), \\ a_{3a} &= T_1\left(f_1 f_0 + f_3 R_{22} + f_2 R_{21}\right), \\ a_{3b} &= -T_2\left({R_{11}}^3 + 2 f_1 R_{12} + f_2 R_{22}\right), \\ a_{4a} &= T_1\left(f_1 + f_3\right)\left({R_{11}}^2 + 2 f_2 + {R_{22}}^2\right), \\ a_{4b} &= -T_2\left(R_{12} f_4\left(f_1 + f_3\right) + \left({R_{11}}^2 + f_2\right)^2\right), \\ a_{div} &= B_{udL}\left(R_{12}{T_2}^2 - R_{21}{T_1}^2 + R_{11}T_1T_2 - R_{22}T_1T_2\right) \end{aligned} \tag{A.6}$$

and the parameters for the calculation of k_{r2}, in (A.4), are given by

$$\begin{aligned} b_0 &= T_1, \\ b_1 &= T_1 R_{22} - T_2 R_{12}, \\ b_2 &= T_1\left({R_{22}}^2 + f_2\right) - T_2\left(f_5 + f_6\right), \\ b_{3a} &= T_1\left({R_{22}}^3 + 2 f_2 R_{22} + f_1 R_{12}\right), \\ b_{3b} &= -T_2\left(f_5 R_{11} + 2 f_5 R_{22} + f_2 R_{12}\right), \\ b_{4a} &= T_1\left(f_2\left({R_{11}}^2 + 2 f_4 + {R_{22}}^2\right) + \left({R_{22}}^2 + f_2\right)^2\right), \\ b_{4b} &= -T_2\left(f_5 + f_6\right)\left({R_{11}}^2 + 2 f_2 + {R_{22}}^2\right), \\ b_{div} &= B_{udL}\left(R_{12}{T_2}^2 - R_{21}{T_1}^2 + R_{11}T_1T_2 - R_{22}T_1T_2\right) \end{aligned} \tag{A.7}$$